Waveguides in finite-height two-dimensional photonic crystals

M. Kafesaki

Institute of Electronic Structure and Laser, Foundation for Research and Technology—Hellas, P.O. Box 1527, 71110 Heraklion, Crete, Greece

M. Agio

Istituto Nazionale per la Fisica della Materia—Dipartimento di Fisica "A. Volta," Università degli Studi di Pavia, via Bassi 6, I-27100 Pavia, Italy, and Ames Laboratory and Department of Physics and Astronomy, Iowa State University, Ames, Iowa 50011

C. M. Soukoulis

Institute of Electronic Structure and Laser, Foundation for Research and Technology—Hellas, P.O. Box 1527, 71110 Heraklion, Crete, Greece, and Ames Laboratory and Department of Physics and Astronomy, Iowa State University, Ames, Iowa 50011

Received December 17, 2001; revised manuscript received April 15, 2002

We present a three-dimensional (3-D) finite-difference time-domain (FDTD) analysis of the transmission and the waveguiding properties of dielectric structures of finite height. A two-dimensional (2-D) photonic-crystal geometry is used for lateral confinement, and traditional waveguiding by dielectric mismatch is used for vertical confinement. We investigate different types of waveguide in photonic crystals with a finite height. We examine the dependence of the guiding properties on the lengths of the holes that constitute the photonic crystal and the widths of the layers of the waveguide. The role of the filling ratio of the holes and the dielectric constants of the upper and the lower layers for the guiding properties is presented. Also, a comparison between the 3-D and the 2-D FDTD results is given. © 2002 Optical Society of America

OCIS codes: 230.7370, 130.2790, 160.3130, 250.5300.

1. INTRODUCTION

The discovery of photonic crystals[1–4] (PCs), i.e., periodic dielectric structures that exhibit bandgaps in their spectra, has opened new ways for efficiently controlling the propagation of light. Examples of such structures are PC waveguides,[5,6] i.e., the guides formed as linear defects in PC structures. Light in the PC waveguides is confined to, and guided along, the one-dimensional channel because the PC prevents light from escaping into the bulk crystal. This property allows light to bend through sharp corners.[7–13]

However, it is still difficult to fabricate three-dimensional (3-D) structures at optical wavelengths.[4,14,15] Recently, full confinement of electromagnetic waves in the microwave region was demonstrated experimentally by use of a layer-by-layer structure.[11,16] Although Noda *et al.*[14] fabricated a 3-D sharp-bend waveguide in the layer-by-layer structure at optical wavelengths, no measurements have been reported yet. Because fabrication of 3-D photonic crystals at optical wavelengths is still a difficult process, an alternative method has been proposed.[17–29] A three-layered dielectric structure is created in the vertical direction, with the central layer having a higher dielectric constant than the upper and the lower dielectric layers. In such a structure light is confined in the vertical direction by traditional waveguiding with dielectric index mismatch and in the lateral direction by the presence of a two-dimensional (2-D) photonic crystal. Two kinds of structure have been used: one in which the upper and the lower dielectric layers are air and another in which the upper and the lower dielectric layers have dielectric constants that are smaller than that of the central layer but much greater than 1. The first structure is called a self-supported membrane, and the second is referred to as a regular waveguide. Which structure has lower losses has not yet been resolved.[30] It is clear, however, that for optoelectronic applications the membrane-based PCs might be not easy to use. It is therefore of considerable importance to find out what type of structure has the lowest losses and produces the best efficiency of bends.

In this paper, we present a detailed finite-difference time-domain (FDTD) analysis of finite-height waveguides. The structures that we analyze consist, in most cases, of three layers of dielectric materials (see Fig. 1). The central layer is chosen to have a high dielectric constant, corresponding to that of either GaAs or GaInAsP. The upper and the lower layers are either identical, to simulate a symmetric waveguide, or different, to simulate an asymmetric guide. The width of the layers is varied. These three-layered waveguide slabs are patterned with a triangular lattice of air holes of vari-

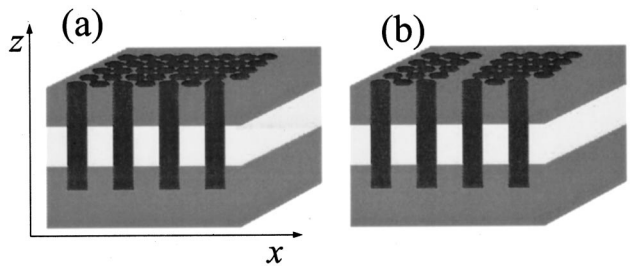

Fig. 1. Three-layer waveguide slab with (a) a PC and (b) a W1 guide (a PC waveguide formed by removing one row of holes from the PC).

able depth. The role of the depth of the holes and their filling ratio in waveguiding and in out-of-plane losses is examined. In addition, the transmission properties of waveguides for which one line of air holes in missing [see Fig. 1(b)] are studied. Finally, a comparison of the 2-D and the 3-D FDTD results is given.

The paper is organized as follows: In Section 2, we present the parameters of our structures and explain the FDTD numerical method that is used to solve Maxwell's equations. We discuss the role of the source and correct detection on the transmission coefficient. In Section 3, we present the results for the cases examined: (a) a GaAs slab sandwiched between air on the top and Al_xO_y on the bottom, (b) a GaAs slab sandwiched between two identical thick layers of $GaAl_{80}As$, and (c) a GaInAsP slab sandwiched between two (different in thickness) layers of InP. In all these cases a 2-D hexagonal lattice of circular air holes was etched. We vary the depth and the radius of the holes such that we can investigate the performance and the guiding properties of the waveguides. In Section 4, we present a comparison of the 3-D results with an effective 2-D system, and, finally, in Section 5, we briefly sum up our results.

2. GEOMETRY AND THE NUMERICAL METHOD

In Fig. 1, we present a view of a three-layer dielectric waveguide. In Fig. 1(a) a three-layer slab waveguide is used to provide vertical confinement of the wave. In Fig. 1(b) there is 3-D confinement: vertically because of the three-layer slab and horizontally because of the PC waveguide formed by the filling of one row of air holes of the PC. In the present paper, we call this PC guide a W1 guide.

Inasmuch as we are interested in guiding properties, we employ the FDTD method in our studies. The FDTD enables us to obtain the transmission coefficient easily through finite slabs of the structures studied and thus to reproduce the results of real experiments.

For the implementation of the FDTD, we follow Yee's algorithm, which is described in detail in Ref. 31. We start from the two Maxwell equations

$$\nabla \times \mathbf{E} = -\mu\mu_0 \frac{\partial \mathbf{H}}{\partial t},$$

$$\nabla \times \mathbf{H} = \epsilon\epsilon_0 \frac{\partial \mathbf{E}}{\partial t}, \tag{1}$$

where ϵ is the modulated dielectric constant, μ is the magnetic permeability, and ϵ_0 and μ_0 are the vacuum permittivity and permeability, respectively. For simplicity, we assume that the dielectric medium is lossless (ϵ is real), and we fix the magnetic permeability (μ) to 1. (It should be mentioned that, even though we use only two of Maxwell's equations, the numerical solutions satisfy all four of Maxwell's equations.[31]) In the framework of the FDTD the real space is discretized in a cubic grid that stores the dielectric constant and the field (**E** and **H**) components. The space and the time derivatives are replaced by central differences, and by use of a finite time step the fields are recursively updated on every grid point. The FDTD algorithm thus reproduces numerically the propagation of the electromagnetic field in real space and time through the waveguide structure.

Because it is not possible to extend the computational system to whole space, we truncate the grid soon after the PC structure and, at the edges, to prevent backreflection, we update the fields by using Liao boundary conditions.[32]

In the research reported here, we choose a computational mesh with a pitch of 1/14th of the PC lattice constant in the xy plane and of 1/14th of the thinner layer in the z direction (unless otherwise explicitly stated). This pitch is approximately 1/14th of the wavelength of interest, which guarantees satisfactory accuracy. The 3-D algorithm places stronger requirements on computational memory and time. The computer memory required for these 3-D calculations is proportional to $N_xN_yN_z$, where N_i ($i = x, y, z$) is the number of grid cells in each direction.

Special attention is paid to the choice of an appropriate source, as our aims are to avoid the excitation of leaky modes that are lost in the top layer and in the substrate and to excite only the fundamental guided mode of the unpatterned slab. To achieve our objectives, we use a spatially extended source covering the entire plane perpendicular to the propagation direction. The source field has a Gaussian spatial profile and is a pulse with a Gaussian envelope in the time domain. As we are interested in transmission properties, by using a pulse, we are able to cover a wide range of frequencies simultaneously. To introduce the source into the calculation, we use the total-field–scattered-field formulation (see Ref. 31, p. 111): We divide the space into two distinct regions separated by a plane of grid points that is perpendicular to the propagation direction. On one side of such a plane Yee's algorithm operates on the total field vector components, and on the other side it operates on only the scattered-field vector components. The source is added onto that plane in the form of incident **E** and **H**. If we assume that y is the propagation direction, the incident **E** component has the form

$$\begin{aligned} E_{\mathrm{inc}}(x, y, z, t) &= \sin\{\omega[ny_0/c - (t - t_0)]\} \\ &\quad \times \exp\{-b_t{}^2[ny_0/c - (t - t_0)]^2\} \\ &\quad \times \exp[-b_x{}^2(x - x_0)^2]\exp[-b_z{}^2(z - z_0)^2]. \end{aligned} \tag{2}$$

The parameters x_0 and z_0 define the centers of the Gaussians in the xz plane, and b_x and b_z are the corre-

sponding widths. y_0 marks the position of the source in the propagation direction (usually a half-lattice constant before the PC), ω is its central angular frequency, t_0 is a time parameter such that the pulse does not reach its maximum value immediately, b_t determines the width of the pulse in the time as well as in the frequency domain, and $n = \sqrt{\epsilon}$ is the refractive index of the medium. The source described above gives beams with satisfactory directionality; thus only a small amount of power moves away from the desired direction. In all the cases that we present here, we have considered a TE incident wave; i.e., the incident electric field is parallel to the layers ($E_{\text{inc}} = E_x$). The incident magnetic field is obtained from $\mathbf{H}_{\text{inc}} = [n/(\mu\mu_0 c)](\hat{j} \times \mathbf{E}_{\text{inc}})$, where $\hat{j}$ is the unit vector in the propagation direction.

The numerical simulation consists of sending the input pulse into the waveguide structure and obtaining the electric and the magnetic field components as functions of time at certain points (detectors) at the beginning and at the end of the waveguide structure. Then the field components are transformed into the frequency domain by use of a fast Fourier transform, and the Poynting vector is calculated. The transmission is given by the ratio of the outgoing and the incident Poynting vectors (the vector's component that is parallel to the propagation direction). It must be mentioned that in calculation of the transmission though a PC structure, the incident Poynting vector is calculated without the presence of the PC (to avoid mixing of incident and reflected waves). For the detection of the fields, we use approximately 100 point detectors that cover almost all the *xz* face of the slab. The outgoing and the incident Poynting vectors are obtained as the averages of the Poynting vectors of all the detectors.

3. RESULTS

In this section, we present results for the three cases studied.

A. Case A: GaAs Slab Waveguide with Air Cladding on the Top and Al_xO_y on the Bottom

The first case is that which was studied by the Sandia and the MIT groups.[23–25] The GaAs layer has a width of 200 nm, with a dielectric constant of $\epsilon = 11.56$. For the bottom layer (Al_xO_y with practically infinite width) $\epsilon = 2.25$. Al_xO_y is converted from $Al_{0.9}Ga_{0.1}As$ by wet oxidation.[23–25] The computational cell in our calculation consists of 8×8 unit cells.

To check whether indeed our incident pulse is close to a waveguide mode[10,12,26,33–35] of the layered heterostructure (without air holes), first, we present the results for the absolute value of the electric field over a *yz* cross section of the slab at two different times, t_1 and t_2. From Fig. 2, we can clearly see that the profile of the incident pulse remains the same as the pulse propagates along the waveguide, as we can verify quantitatively by calculating the *y* component of the Poynting vector, S_y, close to the source and at the other end of the waveguide. From Fig. 3, we can see that, indeed, the ratio of these Poynting vectors is close to 1 for all the frequencies a/λ, where λ is the incident vacuum wavelength and $a = 400$ nm.

Thus both the spatial and the temporal widths of the source describe our system well. The next important test is to see whether our pulse retains its shape as it encounters the 2-D hexagonal PC. This PC has a lattice constant of $a = 400$ nm and an air-filling factor of $f = 32.6\%$ [$f = (2\pi/\sqrt{3})r^2/a^2$, where r is the radius of the holes], and the depth d_s of the holes into the Al_xO_y substrate is $d_s = 300$ nm. These parameters were chosen to give a photonic bandgap (PBG) within the guided-mode region.[23–26,29] In Fig. 4, we present the field $|\mathbf{E}|$ over a *yz* cross section of the slab waveguide, but now with the air holes, at time t_2.

In this case, because of the air holes, there is scattering, and the pulse does not retain its shape. However, there is still mostly propagation in the central (guiding) layer, and the losses are due to the mode mismatch between the PC mode and the incident guided mode of the unpatterned slab. By taking the Fourier transform of the fields, we can calculate the transmission coefficient (as was described in Section 2). In Fig. 5 (dashed curve), we present the transmission coefficient plotted versus the dimensionless frequency a/λ for propagation over the ΓK direction. We can clearly see the width of the PBG. The position as well as the width of this gap are in very good agreement with the corresponding experimental values.[23–25] Forming a W1 guide in this PC and calculating the transmission, we obtain what is shown by the

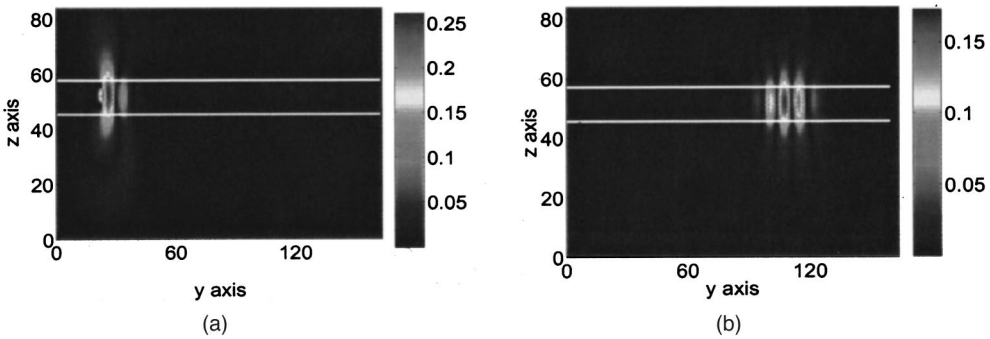

Fig. 2. Field $|\mathbf{E}|$ over a *yz* cross section of the layered structure described for case A (without a PC) at two different times [$t_1 = t_0$ (top) and $t_2 = 2t_0$ (bottom); $t_0 \approx 28 \times 10^{-15}$ s]. Horizontal lines show the layer interfaces. The units on the axis are grid cells (d*y*,d*z*): d$y = a/13$, d$z = a/26$; $a = 400$ nm.

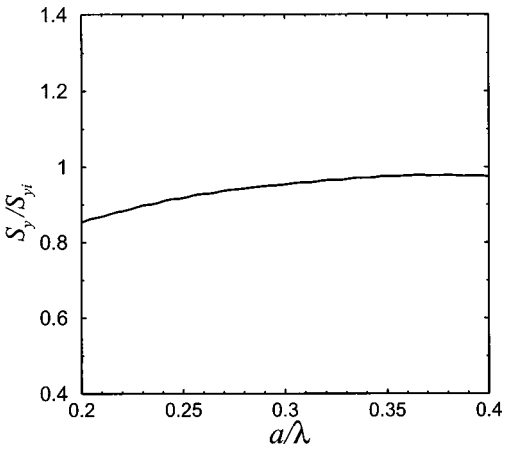

Fig. 3. (Normalized) component of the Poynting vector in the direction of propagation (y) for the layered structure described for case A (without a PC). S_{yi} is the component close to the source, and S_y is the component away from the source. λ is the free-space wavelength, and $a = 400$ nm.

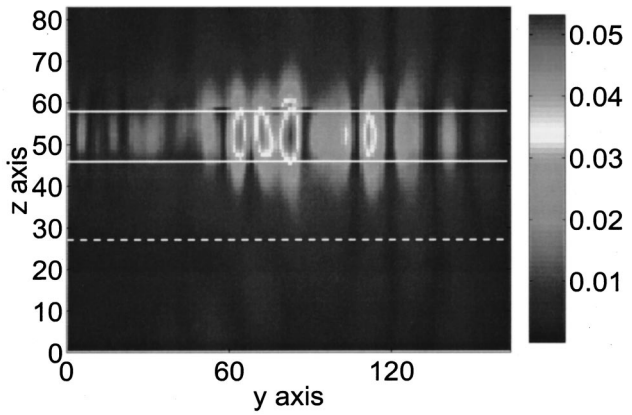

Fig. 4. Field $|\mathbf{E}|$ over a yz cross section of the structure described for case A (three-layer structure with a PC) at $t = 56 \times 10^{-15}$ s. Solid horizontal lines show the layer interfaces; dashed line shows the bottom of the air holes. The units on the axis are grid cells; for the y axis 1 grid cell = dy = $a/13$; for the z axis dz = $a/26$. a is the lattice constant (400 nm). Our computational cell consists of eight lattice constants in the propagation direction and eight in the perpendicular direction.

solid curve of Fig. 5. It is easy to see that transmission through the W1 guide is quite high for almost the entire frequency regime of the PC gap.

B. Case B: GaAs Slab Waveguide with $GaAl_{80}As$ Semiconductor Cladding on Both Sides

In the second case the width of the GaAs layer is 220 nm, with a dielectric constant of $\epsilon = 12.336$. The width of the cladding is practically infinite, with $\epsilon = 9.634$. The lattice constant of the triangular lattice formed by the air holes is $a = 420$ nm, and the air-filling factor is $f = 40\%$. In our calculations the computational cell consists of seven lattice constants a in the propagation direction (ΓK direction) and nine lattice constants $a\sqrt{3}/2$ in the perpendicular direction.

Here, because the refractive-index contrast between the guiding layer and the claddings is low, the guided mode of the layered heterostructure (with no air holes) is not strongly confined in the guiding layer (as in case A). This can be seen from Fig. 6 in which we present the field $|\mathbf{E}|$ over a yz cross section of this layered heterostructure at a specific time.

Again, we use a Gaussian pulse that approximates the guided mode of the unpatterned waveguide, which is weakly confined in the GaAs layer. This approach is used to minimize the excitation of leaky modes. From a triangular array of air holes in the heterostructure, we obtain either a PC or a W1 waveguide. This system does not support truly (lossless) guided modes in the PBG region.[29] Therefore a PC mode propagating through the heterostructure will undergo out-of-plane losses. The transmission through the PC and the W1 for $d_s = 400$ nm has the form shown in Fig. 7(a). As we move to hole depths larger than 400 nm, the transmission increases, although not much.

Our next step is to compare the transmission for cases A and B as it relates to the presence of the PBG structure. We cannot do so by directly comparing the transmissions shown in Figs. 5 and 7(a) because in both figures the losses are due not only to the PC but also to mode mismatch. For both cases A and B there are two occurrences

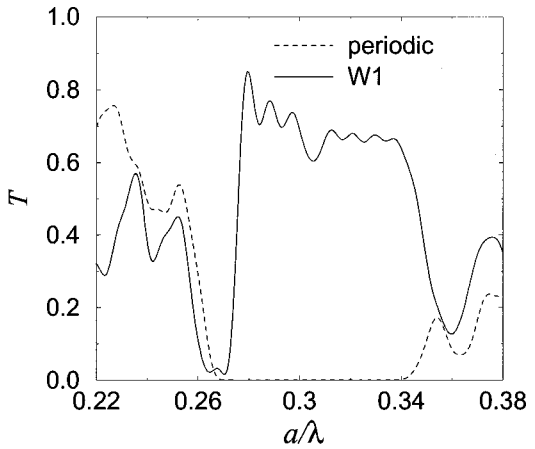

Fig. 5. ΓK transmission coefficient T plotted versus dimensionless frequency a/λ for the three layer structure that is described for case A with a PC (dashed curve) and with a PC with a W1 guide (solid curve). a is the lattice constant, and λ is the free-space wavelength.

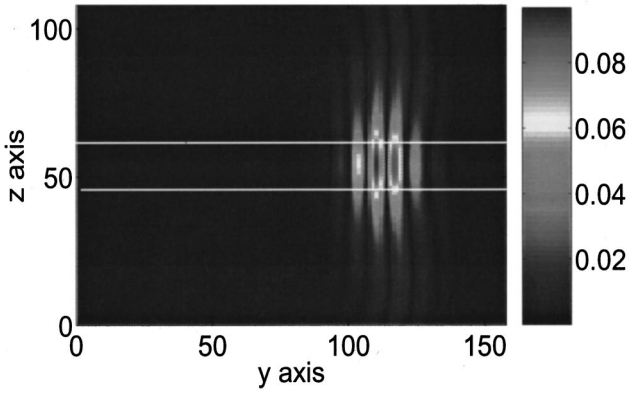

Fig. 6. Field $|\mathbf{E}|$ over a yz cross section of the layered structure described for case B (three-layer structure without a PC) at $t = 15 \times 10^{-15}$ s. Horizontal lines show the layer interfaces. The units on the axis are grid cells (dy,dz): dy = $a/14$, dz = $a/28$; $a = 420$ nm.

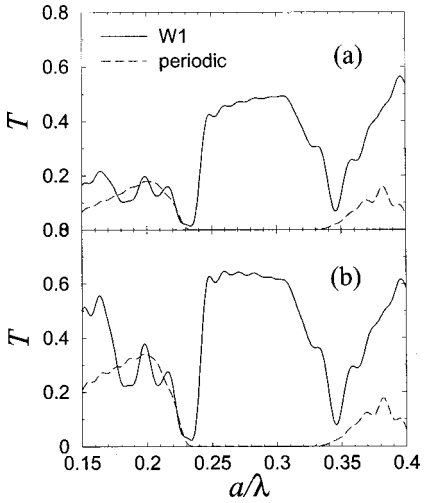

Fig. 7. (a) ΓK transmission coefficient (T) versus dimensionless frequency a/λ for the structure described for case B. The source is a Gaussian pulse with a vertical profile that approximates the layers' guided-mode profile. Dashed curve shows the transmission for a PC; solid curve shows the transmission for a PC with a W1 guide. The cylinder's depth in the substrate is 400 nm. a is the lattice constant, and λ is the free-space wavelength. (b) Same as in (a) but here we calculate the transmission by normalizing the transmitted power by the power transmitted through the layered heterostructure (the structure without PBG material).

of mode mismatch: one for the transition Gaussian source–guided mode of the unpatterned waveguide and the other for the input–output of such a guided mode to and from the PC or the W1. Each mode mismatch causes reflection and out-of-plane losses. We decided to compare cases A and B, eliminating only the effect of the coupling Gaussian source–guided mode. We can do this by calculating the transmission T, using a different normalization: normalizing the transmitted power not by the incident power but by the power transmitted through the unpatterned heterostructure. Using this normalization, we obtain, for case A, a result similar to that of Fig. 5, whereas, for case B, the result is what is shown in Fig. 7(b). Note that the T given in Fig. 7(b) is considerably higher than that presented in Fig. 7(a). Comparing Figs. 7(b) and 5, we see that the two transmissions are comparable. This is an interesting result, which suggests that one can obtain appreciable transmission by patterning the PBG structure in a three-layer system with comparable dielectric constants (as in case B).

C. Case C: GaInAsP Slab Waveguide with InP Semiconductor Cladding on Both Sides

In case C the central layer is GaInAsP; its width is 434 nm, and its dielectric constant is $\epsilon = 11.2225$. The bottom InP layer has a practically infinite width, and $\epsilon = 10.0489$. The top InP layer has a width of 200 nm and is covered by air ($\epsilon = 1$). The lattice constant of the PC is $a = 420$ nm, and the depth of the air holes inside the InP substrate is either 400 or 600 nm. The computational cell in our calculations consists of seven lattice constants in the propagation direction (ΓK) and nine in the perpendicular direction. We studied three air-filling factors f: 30%, 40%, and 45%. As for case B, this PC does not support truly (lossless) guided modes in the PBG region.[29]

In all the cases studied, we used as the incident wave a Gaussian pulse whose vertical spatial profile approximates the profile of the guided mode of the layered heterostructure. The approximation of the guided-mode profile with a Gaussian cannot be good in this case because the guided mode is slightly asymmetric. The air layer above the thin top layer leads to stronger confinement of the wave above than below the guiding layer, as one can see from Fig. 8(a), in which we show the absolute electric field over a yz cross section of the layered heterostructure (with no air holes). In Fig. 8(b) we show the Poynting vector component in the direction of propagation both close to the source and away from the source for this structure. The proximity of the two curves in Fig. 8(b) shows that, despite the asymmetry of the guided mode, its approximation to a Gaussian is not bad.

Forming a PC of air holes (in triangular arrangement) with $f = 40\%$ and plotting the electric field for a hole depth in the substrate of 400 nm, we see that there is a considerable amount of wave that is lost in the sub-

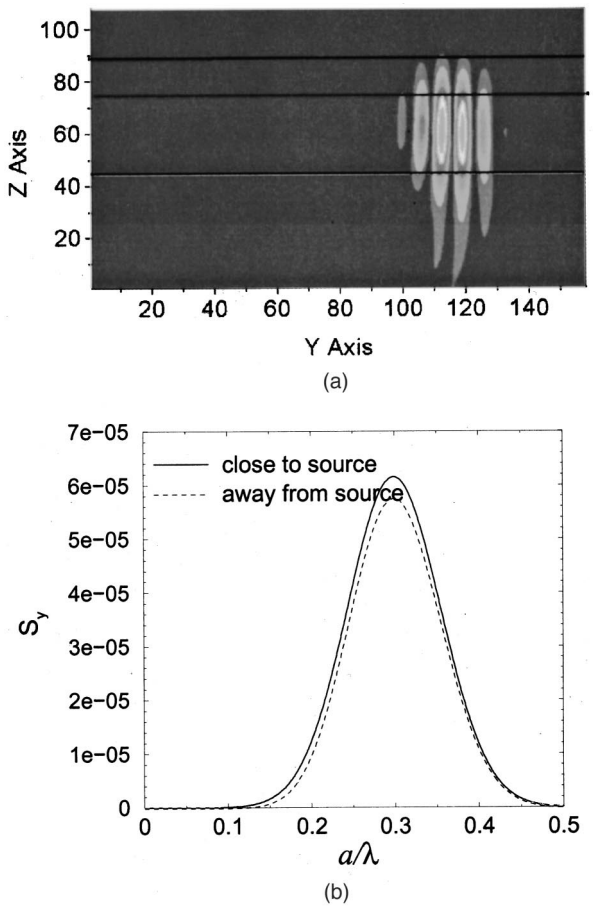

Fig. 8. (a) Field $|\mathbf{E}|$ over a yz cross section of the layered structure described for case C (without a PC) at time $t = 80 \times 10^{-15}$ s. Horizontal lines show the layer interfaces. The units on the axis are grid cells (dy,dz): $dy = a/14$, $dz = a/28$; $a = 420$ nm. (b) Poynting vector component in the propagation direction close to the source and away from the source for the system described for (a).

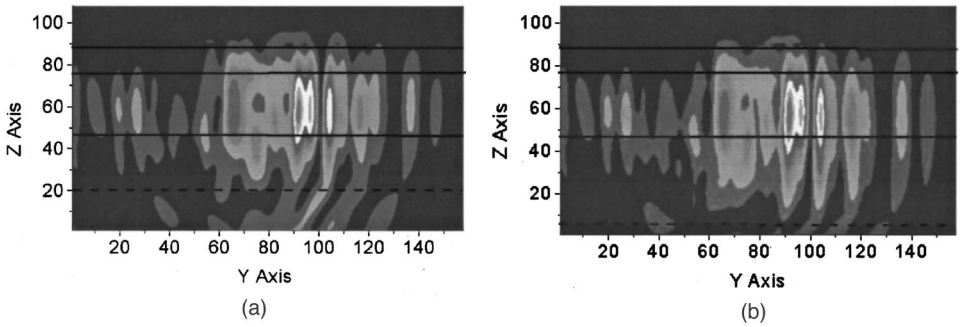

Fig. 9. Field $|\mathbf{E}|$ over a yz cross section of the layered structure described for case C (with a PC) at time $t = 60 \times 10^{-15}$ s. Solid horizontal lines indicate layer interfaces. Dashed horizontal lines indicate lengths of the holes. The hole depth in the InP substrate is (a) $d_s = 400$ nm and (b) $d_s = 600$ nm. The units on the axis are grid cells (dy,dz): d$y = a/14$, d$z = a/28$; $a = 420$ nm.

strate in the form of leaky modes [Fig. 9(a)]. Making the holes 200 nm deeper results in a reduction of the losses, as can be seen from a comparison of Fig. 9(a) with Fig. 9(b). This can also be verified quantitatively by calculation of the corresponding transmission coefficients. In Fig. 10(a), we present the ΓK transmission coefficient for a PC and for a W1 guide for holes 400 nm deep in the substrate; in Fig. 10(b) this depth is 600 nm. Comparing Figs. 10(a) and 10(b), we can see that going from 400 to 600 nm increases the transmission (owing to the decrease of the out-of-plane losses), especially in the lower-frequency regimes.

In Fig. 11, we show the yz (vertical) profile of the guided wave for a W1 guide in a PC of $f = 40\%$ for $d_s = 600$ nm. Here again we see the asymmetry of the guided mode with respect to the center of the guiding layer and the fact that the power that is lost in the substrate is greater than the power lost in air.

Calculating the transmission coefficient for the InP system and for air-filling ratios f that are different from 40%, we found that the optimum f for broadband and considerable guiding is 40%–45%. In Fig. 12, we show the ΓK transmission for $f = 30\%$ [Fig. 12(a)] and for $f = 45\%$ [Fig. 12(b)], both for $d_s = 600$ nm.

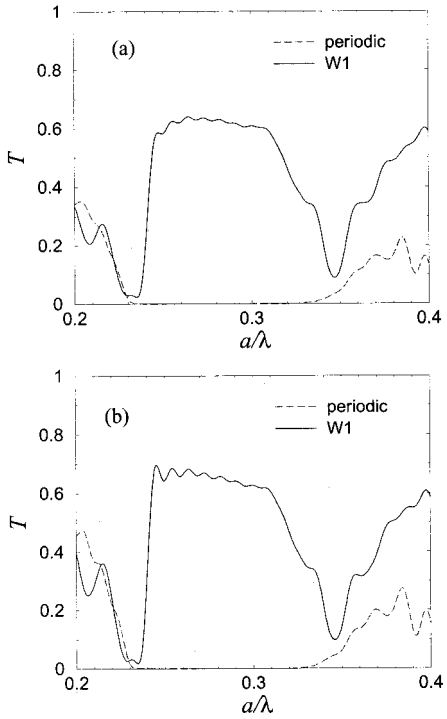

Fig. 10. ΓK transmission coefficient T versus dimensionless frequency a/λ for the structure of case C, with an air filling ratio of $f = 0.4$. Dashed curves show the transmission for a PC; solid curves show the transmission for a PC with a W1 guide. The cylinder's depth in the substrate is 400 nm for (a) and 600 nm for (b). a is the lattice constant, and λ is the free-space wavelength.

4. COMPARISON OF TWO-DIMENSIONAL AND THREE-DIMENSIONAL RESULTS

Obtaining numerical results by use of the 3-D FDTD method is time and memory consuming. Therefore it would be very interesting and useful if one could approximate the 3-D problem of the finite-height cylinders with a 2-D model (infinite-height holes).

To this purpose,[13] we have to consider a host material with an effective refractive index (equal to the refractive index of the guided mode of the layered heterostructure; this condition accounts for the fact that there is guiding in the vertical direction as a result of the presence of different layers) and a loss parameter for the holes (to represent the out-of-plane losses). The loss parameter can be an imaginary part in the holes' dielectric constant or,

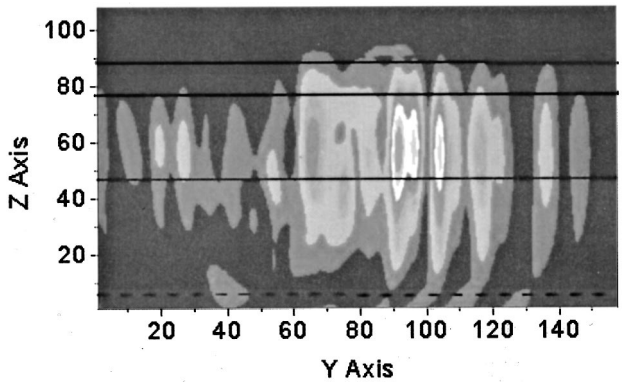

Fig. 11. Field $|\mathbf{E}|$ over a yz cross section of the structure described for case C (layered structure with a W1 guide) at time $t = 80 \times 10^{-15}$ s. Solid horizontal lines show the layer interfaces. Dashed horizontal line shows the depth of the holes. The holes' depth in the InP substrate is $d_s = 600$ nm. Units on the axis are grid cells (dy,dz): d$y = a/14$, d$z = a/28$; $a = 420$ nm.

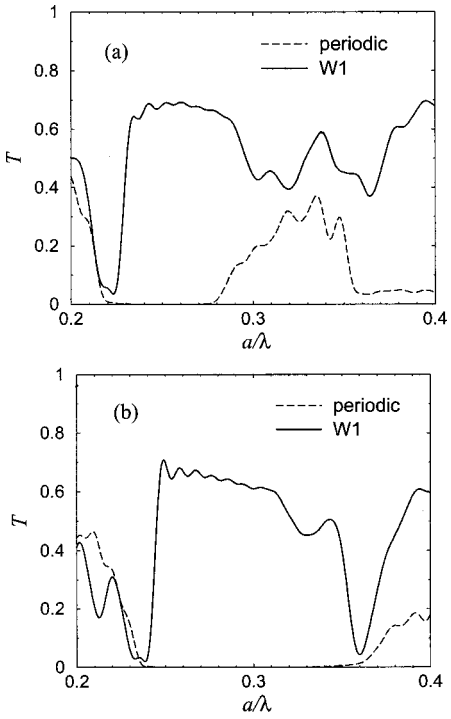

Fig. 12. ΓK transmission coefficient T versus dimensionless frequency a/λ for the structure of case C, with air-filling ratios of (a) $f = 0.3$ and (b) $f = 0.45$. Dashed curves show the transmission for a PC; solid curves show the transmission for a PC with a W1 guide. The holes' depth in the substrate is 600 nm. a is the lattice constant, and λ is the free-space wavelength.

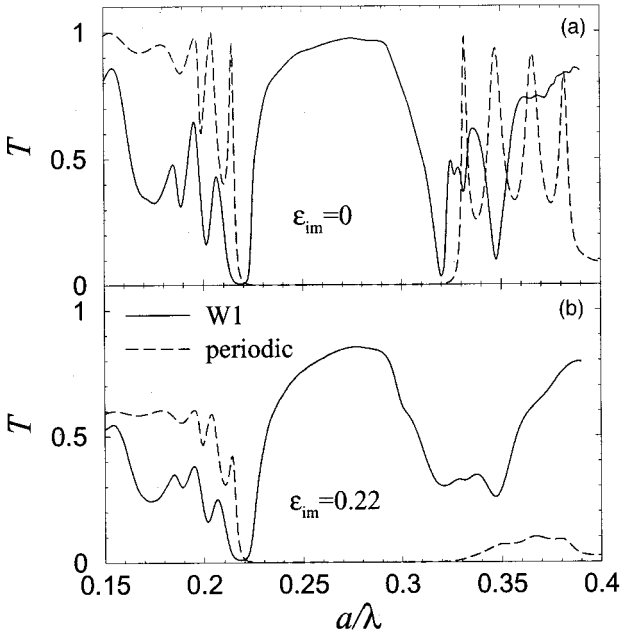

Fig. 13. ΓK transmission coefficient T plotted versus dimensionless frequency a/λ for a system of infinite air cylinders (with dielectric constant $1 + i\epsilon_{im}$) in a host with $\epsilon = 11.56$. (a) $\epsilon_{im} = 0$, (b) $\epsilon_{im} = 0.22$. Dashed curves show the transmission for a periodic system; solid curves show the transmission for a W1 guide. a is the lattice constant, and λ is the free-space wavelength. The air-filling ratio is $f = 0.4$, and the grid's pitch is $a/34$.

equivalently, a finite conductivity.[30] In what follows, we present 2-D FDTD results based on the above considerations for the systems described for cases B and C. We compare them with the corresponding 3-D results and examine how and to what extent a 2-D calculation can replace a 3-D calculation.

For the GaAs structure of case B the effective dielectric constant that we use for the 2-D calculations is $\epsilon = 11.56$. The 2-D FDTD results for the transmission through a triangular periodic lattice and through a W1 guide are shown in Fig. 13. For the InP structure of case C, $\epsilon = 10.5$, and the 2-D FDTD results are shown in Fig. 14.

In the 2-D calculations for the purely periodic case, we use a source with a constant profile in the direction perpendicular to the propagation and in Bloch's boundary conditions at the boundaries parallel to the propagation direction. For W1 the source is the output of a ridge access guide of width $w \approx 1.1a$ (note that this kind of source cannot be used in 3-D calculations because of the large memory requirements). For both the W1 and the periodic cases, the computational cell consists of seven air cylinders in the propagation direction, and the pitch of the grid is the 1/34th of the lattice constant.

Comparing Fig. 13 with Fig. 7(a) and Fig. 14 with Fig. 10, we can make the following observations: (a) The 2-D transmission is considerably larger than the corresponding 3-D transmission because no out-of-plane losses are included in the 2-D calculation. (b) With regard to the position and the width of the PBG the approximation of a 3-D calculation with an equivalent 2-D calculation seems to produce extremely good results. The widths of the 3-D and the 2-D gaps are almost the same, and the positions of the gaps are only slightly different. The situation, however, can be further improved, and a simultaneous gap width and position coincidence between 2-D and 3-D results can be achieved. This can be done if we consider, in addition to an effective dielectric constant, an effective air-filling ratio f.[29] In Fig. 15, we present, for the system of case C, the dependence of the upper and the lower edges of the 2-D gap on the air-filling ratio. We can see

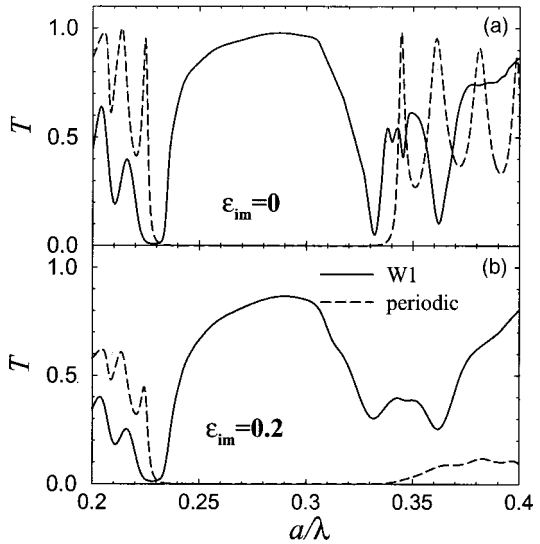

Fig. 14. Same as in Fig. 13 for a host with dielectric constant $\epsilon = 10.5$. (a) $\epsilon_{im} = 0$, (b) $\epsilon_{im} = 0.2$.

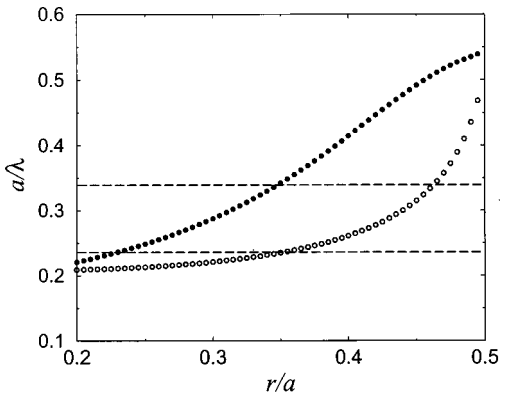

Fig. 15. Upper (filled circles) and lower (open circles) edges of the 2-D gap plotted as a function of ratio r/a for the system shown in Fig. 14. The two gap edges are calculated by the plane-wave method.[2] Dashed horizontal lines show the upper and the lower edges of the 3-D gap for an air-filling ratio of $f = 40\%$.

that, at $r/a \approx 0.35$ ($f \approx 0.44$), both the position and the width of the 2-D gap coincide with those of the 3-D gap for $f \approx 0.40$.

5. CONCLUSIONS

We have numerically studied the transmission and the waveguiding properties of 2-D PC dielectric heterostructures by using a 3-D FDTD method. We have examined systems that exhibit strong (case A) and weak (cases B and C) confinement in the vertical direction. For case A, the PC supports truly guided modes, but the transmission is reduced by mode mismatch (nonoptimal coupling efficiency). For the other two cases the out-of-plane losses are unavoidable. Nevertheless, the transmission can be fairly high, as the etch depth is larger than a critical value (Fig. 10). The transmission coefficient through a W1 waveguide can be as high as 70% [Fig. 11(b)] for the GaInAsP slab waveguide with InP semiconductor cladding on both sides.

Finally, we have compared our 3-D FDTD results with 2-D results that were obtained by use of both an effective index of refraction and an effective filling ratio. Close agreement between the 3-D results and the effective 2-D results was obtained.

ACKNOWLEDGMENTS

We thank M. Sigalas, H. Benisty, and I. El-Kady for useful discussions. The Ames Laboratory is operated for the U.S. Department of Energy by Iowa State University under contract W-7405-Eng-82. This research was supported by the Director for Energy Research, Office of Basic Science (U.S.) and by the European Union Information Societies Technology project "Photonic Crystal Integrated Circuits."

REFERENCES AND NOTES

1. J. D. Joannopoulos, R. D. Meade, and J. N. Winn, *Photonic Crystals—Molding the Flow of Light* (Princeton U. Press, Princeton, N. J., 1995).
2. C. M. Soukoulis, ed., *Photonic Band Gap Materials*, Vol. 315 of NATO Advanced Scientific Institutes Series E, Applied Sciences (Kluwer Academic, Dordrecht, The Netherlands, 1996).
3. Special section on Electromagnetic Crystal Structures, Design, Synthesis, and Applications, A. Scherer, T. Doll, E. Yablonovitch, E. O. Everitt, and J. A. Higgins, eds., J. Lightwave Technol. **17**(11), (1999).
4. C. M. Soukoulis, *Photonic Crystals and Light Localization in the 21st Century* (Kluwer Academic, Dordrecht, The Netherlands, 2001).
5. A. Mekis, J. C. Chen, I. Kurland, S. Fan, P. R. Villeneuve, and J. D. Joannopoulos, "High transmission through sharp bends in photonic crystal waveguides," Phys. Rev. Lett. **77**, 3787–3790 (1996).
6. S. Y. Lin, E. Chow, V. Hietala, P. R. Villeneuve, and J. D. Joannopoulos, "Experimental demonstration of guiding and bending of electromagnetic waves in a photonic crystal," Science **282**, 274–276 (1998).
7. M. M. Sigalas, R. Biswas, K. M. Ho, C. M. Soukoulis, and D. D. Cronch, "Waveguides in photonic band gap materials," paper presented at the Fourteenth Annual Review on Progress and Applications in Computational Electrodynamics, Monterey, Calif., 1998.
8. M. M. Sigalas, R. Biswas, K. M. Ho, C. M. Soukoulis, D. Turner, B. Vasiliu, S. C. Kothari, and S. Lin, "Waveguide bends in three-dimensional layer-by-layer photonic bandgap materials," Microwave Opt. Technol. Lett. **23**, 56–59 (1999).
9. A. Chutinan and S. Noda, "Highly confined waveguides and waveguide bends in three-dimensional photonic crystals," Appl. Phys. Lett. **75**, 3739–3741 (1999).
10. A. Chutinan and S. Noda, "Design for waveguides in three-dimensional photonic crystals," Jpn. J. Appl. Phys., Part 1 **39**, 2353–2356 (2000).
11. M. Bayindir, E. Ozbay, B. Temelkuran, M. M. Sigalas, C. M. Soukoulis, R. Biswas, and K. M. Ho, "Guiding, bending, and splitting of electromagnetic waves in highly confined photonic crystal waveguides," Phys. Rev. B **63**, R-081107 (2001).
12. I. El-Kady, M. M. Sigalas, R. Biswas, and K. M. Ho, "Dielectric waveguides in two-dimensional photonic bandgap materials," J. Lightwave Technol. **17**, 2042–2049 (1999).
13. A. Chutinan and S. Noda, "Waveguides and waveguide bends in two-dimensional photonic crystal slabs," Phys. Rev. B **62**, 4488–4492 (2000).
14. S. Noda, K. Tomoda, N. Yamamoto, and A. Chutinan, "Full three-dimensional photonic crystals at near-infrared wavelengths," Science **289**, 604–606 (2000).
15. S. Lin and J. G. Fleming, "A three-dimensional optical photonic crystal," J. Lightwave Technol. **17**, 1944–1947 (1999).
16. K. M. Ho, C. T. Chan, C. M. Soukoulis, R. Biswas, and M. Sigalas, "Photonic band gaps in three dimensions: new layer-by-layer periodic structures," Solid State Commun. **89**, 413–416 (1994).
17. T. F. Krauss, R. M. de la Rue, and S. Brand, "Two-dimensional photonic-bandgap structures operating at near-infrared wavelengths," Nature **383**, 649 (1996).
18. D. Labilloy, H. Benisty, C. Weisbuch, T. F. Krauss, R. M. De La Rue, V. Bardinal, R. Houdre, U. Oesterle, D. Cassagne, and C. Jouanin, "Quantitative measurement of transmission, reflection, and diffraction of two-dimensional photonic band gap structures at near-infrared wavelengths," Phys. Rev. Lett. **79**, 4147–4150 (1997).
19. H. Benisty, C. Weisbuch, D. Labilloy, M. Rattier, C. J. M. Smith, T. F. Krauss, R. M. De la Rue, R. Houdre, U. Oesterle, C. Jouanin, and D. Cassagne, "Optical and confinement properties of two-dimensional photonic crystals," J. Lightwave Technol. **17**, 2063–2077 (1999), and references therein.
20. T. Baba, N. Fukaya, and J. Yonekura, "Observation of light propagation in photonic crystal optical waveguides with bends," Electron. Lett. **35**, 654–655 (1999).
21. M. Tokushima, H. Kosaka, A. Tomita, and H. Yamada, "Lightwave propagation through a 120° sharply bent single-line-defect photonic crystal waveguide," Appl. Phys. Lett. **76**, 952–954 (2000).
22. M. Loncar, D. Nedeljkovic, T. Doll, J. Vuckovic, A. Scherer,

and T. P. Pearsall, "Waveguiding in planar photonic crystals," Appl. Phys. Lett. **77**, 1937–1939 (2000).
23. E. Chow, S. Y. Lin, S. G. Johnson, P. B. Villeneuve, J. D. Joannopoulos, J. R. Wendt, G. A. Vawter, W. Zubrzycki, H. Hou, and A. Alleman, "Three-dimensional control of light in a two-dimensional photonic crystal slab," Nature **407**, 983–986 (2000).
24. S. Y. Lin, E. Chow, and S. G. Johnson, "Demonstration of highly efficient waveguiding in a photonic crystal slab at the 1.5-μm wavelength," Opt. Lett. **25**, 1297–1299 (2000).
25. E. Chow, S. Y. Lin, J. R. Wendt, S. G. Johnson, and J. D. Joannopoulos, "Quantitative analysis of bending efficiency in photonic-crystal waveguide bends at $\lambda = 1.55$ μm wavelength," Opt. Lett. **26**, 286–288 (2001).
26. S. G. Johnson, S. Fan, P. R. Villeneuve, J. D. Joannopoulos, and L. A. Kolodziejski, "Guided modes in photonic crystal slabs," Phys. Rev. B **60**, 5751–5758 (1999).
27. T. Ochiai and K. Sakoda, "Dispersion relation and optical transmittance of a hexagonal photonic crystal slab," Phys. Rev. B **63**, 125107 (2001).
28. T. Ochiai and K. Sakoda, "Nearly free-photon approximation for two-dimensional photonic crystal slabs," Phys. Rev. B **64**, 045108 (2001).
29. L. C. Andreani and M. Agio, "Photonic bands and gap maps in a photonic crystal slab," IEEE J. Quantum Electron. (to be published).
30. H. Benisty, D. Labilloy, C. Weisbuch, C. J. M. Smith, T. F. Krauss, D. Cassagne, A. Beraud, and C. Jouanin, "Radiation losses of waveguide-based two-dimensional photonic crystals: positive role of the substrate," Appl. Phys. Lett. **76**, 532–534 (2000).
31. A. Taflove, *Computational Electrodynamics, The Finite Difference Time Domain Method* (Artech House, Boston, Mass., 1995).
32. Liao boundary conditions are based on extrapolation of the fields in space and time by use of a Newton backward-difference polynomial. They are introduced in Z. P. Liao, H. L. Wong, B. P. Yang, and Y. F. Yuan, "A transmitting boundary for transient wave analyses," Sci. Sin., Ser. A **27**, 1063–1076 (1984). Liao boundary conditions are also described in detail in Ref. 31.
33. B. D'Urso, O. Painter, J. O'Brien, T. Tombrello, A. Yariv, and A. Scherer, "Modal reflectivity in finite-depth two-dimensional photonic-crystal microcavities," J. Opt. Soc. Am. B **15**, 1155–1159 (1998).
34. O. Painter, J. Vuckovic, and A. Scherer, "Defect modes of a two-dimensional photonic crystal in an optically thin dielectric slab," J. Opt. Soc. Am. B **16**, 275–285 (1999).
35. A. Mekis, S. H. Fan, and J. D. Joannopoulos, "Bound states in photonic crystal waveguides and waveguide bends," Phys. Rev. B **58**, 4809–4817 (1998).